Hindawi
Advances in Civil Engineering
Volume 2024, Article ID 4618708, 12 pages
https://doi.org/10.1155/2024/4618708

Research Article

Analysis of Traveling Wave and Combined Site Effect of Long-Span Upper-Bearing Concrete-Filled Steel Tubular Arch Bridge

Zite Li,[1,2] **Genhui Wang**,[1] **Jiang Fan**,[2] **Yue Jian**,[3] **and Yongliang Zhang**[1]

[1]*School of Civil Engineering, Lanzhou Jiaotong University, Lanzhou 730070, Gansu, China*
[2]*Gansu Province Transportation Planning, Survey and Design Institute Co. Ltd., Lanzhou 730030, Gansu, China*
[3]*Department of Basic Sciences, Lanzhou Institute of Technology, Lanzhou 730050, Gansu, China*

Correspondence should be addressed to Genhui Wang; wahl@mail.lzjtu.cn

Received 21 October 2023; Revised 9 December 2023; Accepted 27 December 2023; Published 16 January 2024

Academic Editor: Yi Zhang

In order to study the traveling wave effect and combined site effect of long-span steel tube concrete-filled arch bridge, a 400-m span bridge of the same type is taken as an example, and a large-mass time-history analysis method with multipoint input of recorded seismic waves is used. A total of 11 kinds of traveling wave excitations and 9 kinds of combined site excitations under 4 types of typical sites are carried out to calculate the structural response, and the chord axial force ratio and displacement changes are compared and analyzed. The results show that the long-span arch bridge also has nonuniform seismic excitation conditions in the lateral and vertical directions, and the spatial effect of the structural response is significant; under the traveling wave excitation, the change of the axial force ratio of the chord has a certain periodicity, and it is not the larger the axial force ratio is, the larger the axial force ratio is; the X direction has a significant influence, the maximum axial force ratio of the vault under the design condition is 6.26, and the changes in the Y and Z directions are relatively gentle, but there are still nearly two times the working condition; after the same amplitude modulation of different recorded waves, under the uniform excitation, the axial force is similar, but the displacement is quite different; under the unidirectional traveling wave excitation, the displacement in the X and Z directions shows an accelerating and increasing trend toward the vault. When it is relatively consistent under the unidirectional combined site excitation, and the axial force ratio changes under small and then increases, the L/4–3L/8 segment has a significant impact; the axial force ratio changes are the combined site excitation in different directions are spatially random; three under the combined site excitation. The axial force ratio in the orthogonal direction changes greatly. When the hard field is transformed into the soft field, the axial force ratio decreases, and the displacement increases continuously.

1. Introduction

In civil engineering, concrete-filled arch bridge (CFST) constructions have been studied and used for a very long time. The cross-section is a particular kind of steel–concrete combination, where the concrete is packed tightly inside the steel tube, enhancing the tube wall's compressive stability and efficiently utilizing steel's high strength; concurrently, the core concrete is subjected to the tube wall's hoop action, which significantly increases its ductility and compressive strength, making the brittle failure-prone concrete possesses elastic–plastic properties. The composite structure's stress state has changed qualitatively as a result of the performance enhancement [1]. A thrust construction that produces horizontal forces at the arch foot when vertical loads are applied is an arch bridge. The primary load-bearing element is the main arch ring, and it has a high-stress efficiency and completely utilizes the section material's strength in an axial or mild eccentric compression stress state [2]. An effective composite stress system is created by the steel tube concrete arch bridge, which combines the highly efficient composite cross-section with the arch ribs primarily under pressure in structural construction. This makes this kind of bridge more popular [3], and advancements in both the span and quantity of construction have been made with engineering applications across China. More than 490 steel tube concrete arch

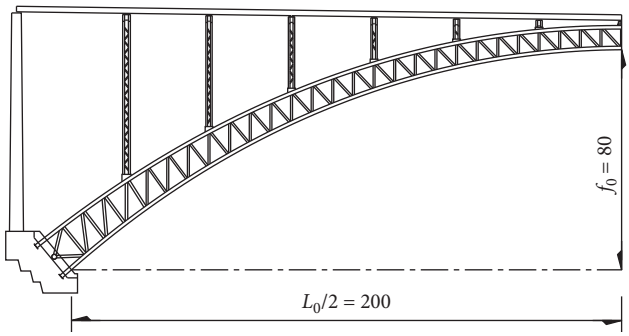

Figure 1: Half main bridge facade (unit: m).

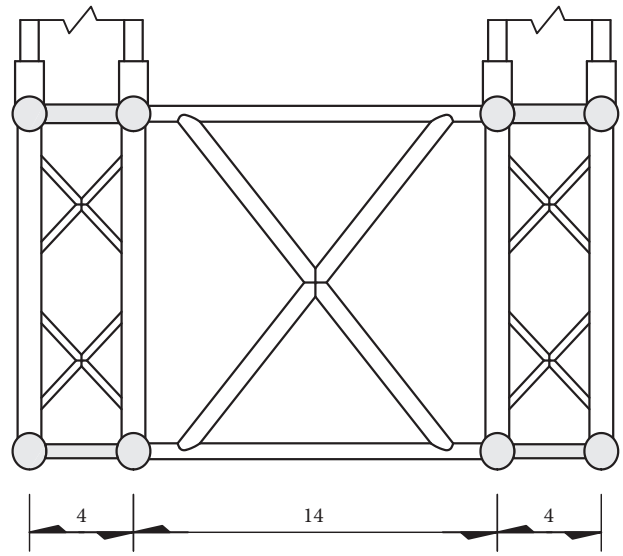

Figure 2: Typical cross-section of the main arch ring (unit: m).

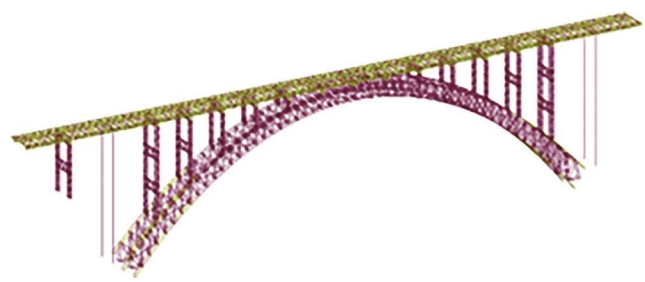

Figure 3: Full bridge finite element model.

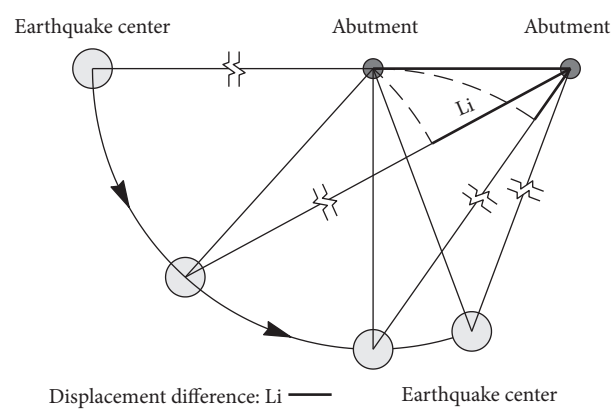

Figure 4: Schematic diagram of in-plane nonuniform excitation.

bridges were under construction and finished in China as of the end of 2022. The Pingnan Third Bridge is a 575-m long through steel tube concrete highway arch bridge that was finished and made operational in 2020. Presently the largest highway and railway steel tube concrete arch bridge in the world, the Zangmu Bridge is a 490 m through steel tube railway arch bridge that was finished and opened to traffic in 2021. The deck-type steel tube concrete truss arch bridge in valleys or canyon areas has exceptional seismic and wind resistance performance, strong permeability, reasonable structural stress, good terrain adaptability, and is relatively less expensive than cable-bearing structures. The type of bridge is highly competitive [4].

The process of ground motion involves a great deal of spatiotemporal variation. Large-span bridge seismic design requires consideration of both the spatial variation characteristics of ground motion as well as its time-varying characteristics [5, 6]. The large-span deck steel tube concrete arch bridge has a greater eccentricity in relation to the arch seat and continuously varies in cross-sectional centroid positions. It stretches simultaneously in both span and height dimensions. When nonuniform inputs are applied, the seismic response becomes more spatial, and the structural mass distribution becomes extremely discontinuous. With the construction of the Pingnan Third Bridge [7], the composite structure of "circular diaphragm wall + reinforced pebble layer" was utilized for the first time as the foundation for long-span arch bridges, establishing a precedent for the building of this kind of bridge in weak strata. As a result, it seems that there is substantial study value to both the combined site effect and the traveling wave effect. Numerous researchers have studied how large-span arch bridges react to nonuniform seismic inputs in the last few years. Through steel truss arch bridges' seismic response to traveling waves was examined using the large mass method in literatures [8, 9]. The results showed that traveling waves have a certain impact on the seismic response of large-span steel arch bridges, and the phase difference increases, and the traveling wave effect becomes more significant; Zhang et al. [10] studied the pseudo static and dynamic components of a 490-m railway steel truss arch bridge under the traveling wave effect, and the results showed that the seismic response of the traveling wave effect was significantly affected; literatures [11–14] analyzed the traveling wave effect of CFST arch bridges, and the results showed that the traveling wave effect has a significant impact on the seismic response of concrete arch bridges, especially on the arch crown section; Wang et al. [15] analyzed the nonuniform seismic response of steel tube concrete arch bridges, and the results showed that the influence of local site effects is greater than that of traveling wave effects and partial coherence effects; Li et al. [16] conducted a study on the dynamic response of a steel tube concrete arch bridge under nonuniform seismic inputs, and the

Table 1: Peak acceleration correction value.

Seismic wave	Main direction peak acceleration (g)	Safety assessment peak acceleration (g)	Correction factor	Abbreviation
EL Centro	0.36	0.415	1.163	E
Taft	0.18		2.315	T
Hollywood	0.06		7.007	H
San Fernando	0.32		1.316	S

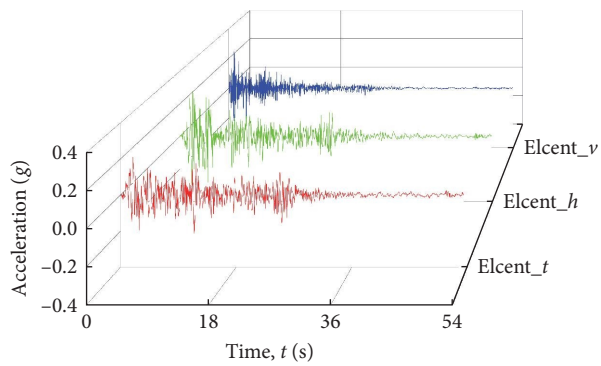

Figure 5: Corrected EL Centro 3D seismic waves.

Table 2: Apparent velocity and delay.

Working condition	1	2	3	4	5	6	7	8	9	10	11	12
Apparent velocity v/(m/s)	150	200	250	375	500	650	800	1200	1600	2000	4000	∞
Delay (t/s)	2.67	2.00	1.60	1.07	0.80	0.62	0.50	0.33	0.25	0.20	0.10	0

results showed that the influence of spatial variability under multidimensional inputs on the seismic reliability of the steel tube concrete arch bridge cannot be ignored; Li et al. [17] used OpenSEES software to artificially synthesize spatially nonuniform seismic waves, and studied the incoherence effect, site effect, and traveling wave effect of ground motion for a continuous beam arch composite bridge. The response of steel tube concrete arch bridges to spatially varying ground motion, including local field effects, was studied by Bi et al. [18]. The traveling wave effect of a through steel tube concrete arch bridge was analyzed using the mass analysis method by Ma et al. [19], and the seismic damping effect of MR dampers under multisupport seismic excitation was examined by Zheng et al. [20]. Soyluk [21] found that the spatial variability effect of seismic waves had a significant influence on the structural response when he investigated the random vibration computation methods for large-span bridges under multipoint excitation. In conclusion, due to the different distances and angles between the arch base and the seismic source, the large-span arch bridge must receive different variations in the frequency spectrum and phase of the seismic input waves. The surface propagation medium is also incredibly unpredictable. The nonuniform seismic input that occurs at the arch base will also have distinct effects on the structural reaction [22, 23].

An example used in this study is a 400-m-deck steel-tube concrete highway arch bridge located in China's northwest seismic area. The structural response calculations were carried out for a total of 11 types of traveling wave inputs and 9 types of combined site inputs for 4 typical sites, using the mass time history analysis method with multiple input points and the typical site recorded waves corrected for effective peak acceleration in the safety assessment report. Analyses of displacement variations and the chord-axial force ratio were carried out, along with studies of the traveling wave and combined site effects of this kind of bridge.

2. Bridge Model and Dynamic Characteristics

2.1. Bridge Overview. A particular highway bridge's basic structure is a 1-net 400-m-long steel tube concrete arch bridge with an arch axis coefficient of 1.55, a net rise height of $f_0 = 80$ m, and a net rise span ratio of $f_0/L_0 = 1/5$. The main arch ring uses a space truss structure with equal width and height variation of four limbs steel tube concrete double arch ribs; the arch crown changes from 7.5 to 14 m at the arch foot; the transverse center distance of the truss ribs is 18 m; Arch rib chord adopts Φ1,300-mm rolled welded steel tube filled with C60 self-compacting shrinkage compensating concrete, with web members made of Φ914 and Φ711 finished seamless steel tube; the bridge deck system uses $(1 \times 40 + 12 \times 30 + 1 \times 40)$ m steel bottom plate corrugated web concrete bridge deck composite beam; the columns on the arch are made of diagonal batten four limb steel tube lattice columns; the arch and abutment adopt an expanded foundation; the construction uses a cable-stayed buckle hanging +

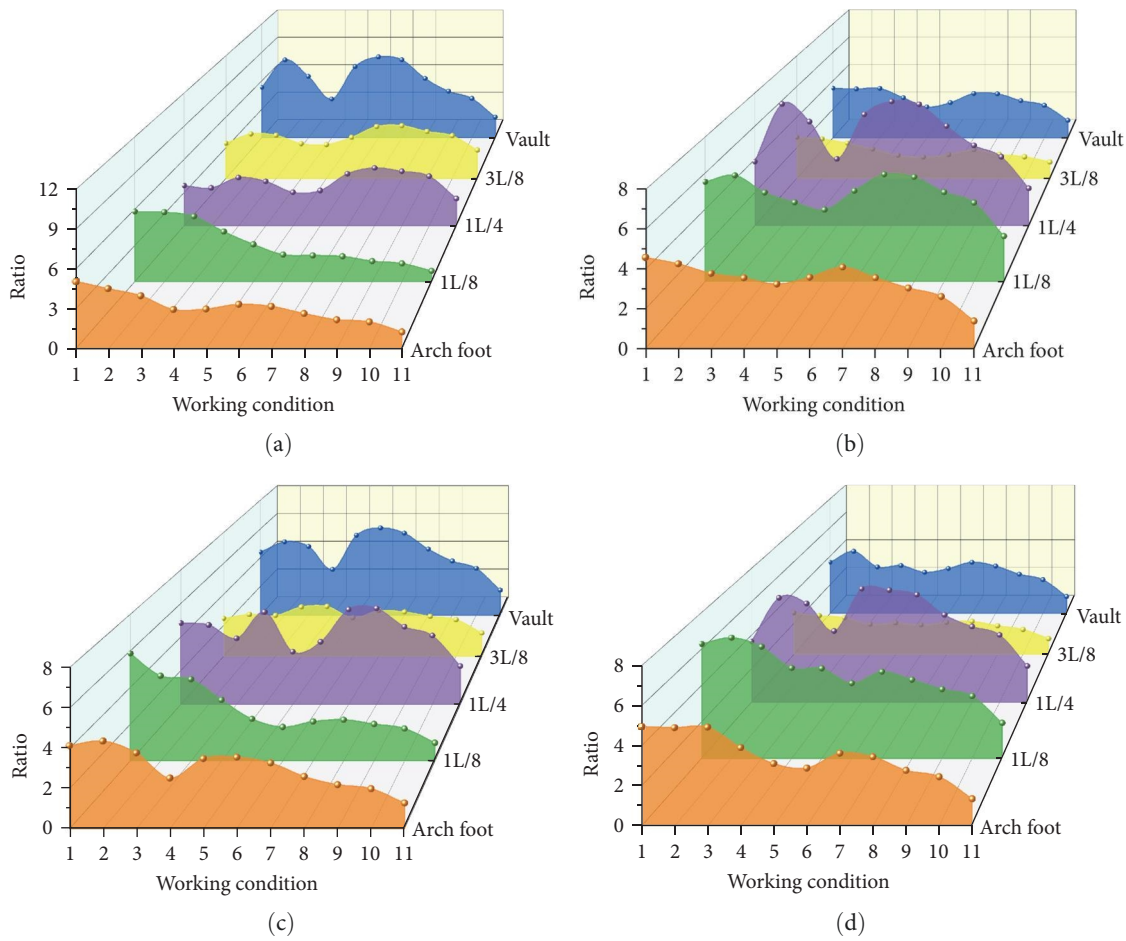

Figure 6: Axial force ratio diagram of chord excited by traveling wave in X direction: (a) upper chord (N_{max}); (b) lower chord (N_{max}); (c) upper chord (N_{min}); (d) lower chord (N_{min}).

cable suction method. the chord uses Q390D; the remaining chord uses Q355D. The horizontal basic seismic peak acceleration is 02 g, the site characteristic period is 0.45 s, the site category is Class I, the fortification intensity is VIII, and the fortification category is Class A. The main bridge's structural layout is depicted in Figures 1 and 2, which show the typical cross-section of the main arch ring.

2.2. Finite Element Model. With MIDAS/CIVIL software, a spatial finite element model for a bridge is created. The combined modulus of the unified theory is used to calculate the axial compression and shear modulus of the steel tube concrete section; the structural mass is concentrated into three directions of space, and a large mass of nodes is added at the constraint of the arch foot; plate elements are used to simulate the bridge deck, while spatial beam elements are used to simulate the remaining members. High-damping rubber bearings are used on the top of the column and the junction pier, while fixed limitations are used on the bottom and arch foot of the pier. As per the stiffness calculation using general connection simulation, the steel tube concrete structure's damping ratio is determined to be 0.03 [24]. The bridge's spatial finite element model is displayed in Figure 3.

3. Dynamic Equation and Seismic Wave Input

3.1. Mass Method Dynamic Equation. By fastening a mass matrix to the structural support nodes, the large mass technique attaches a force time history input to the system [18]. The extra mass M_0 is typically 10^6 times the structure's entire mass. On the support node, the inertial force is transformed into a time-history external force by relaxing the translational displacement constraint in one input direction [16]. The dynamic balance equation is as follows:

$$\begin{bmatrix} \boldsymbol{M}_{ss} & 0 \\ 0 & \boldsymbol{M}_{bb} + \boldsymbol{M}_0 \end{bmatrix} \begin{Bmatrix} \ddot{u}_s \\ \ddot{u}_b \end{Bmatrix} + \begin{bmatrix} C_{ss} & 0 \\ 0 & \boldsymbol{C}_{bb} \end{bmatrix} \begin{Bmatrix} \dot{u}_s \\ \dot{u}_b \end{Bmatrix} + \begin{bmatrix} K_{ss} & K_{sb} \\ K_{bs} & K_{bb} \end{bmatrix} \begin{Bmatrix} u_s \\ u_b \end{Bmatrix} = \begin{bmatrix} 0 \\ F \end{bmatrix} = \begin{bmatrix} 0 \\ \boldsymbol{M}_{ss}\, \ddot{u}_g \end{bmatrix}, \tag{1}$$

where M, C, K is the mass matrix, damping matrix, and stiffness matrix; $\ddot{u}_b, \dot{u}_b, u_b$ is the acceleration, velocity, and displacement of the supporting node; $\ddot{u}_s, \dot{u}_s, u_s$ is the

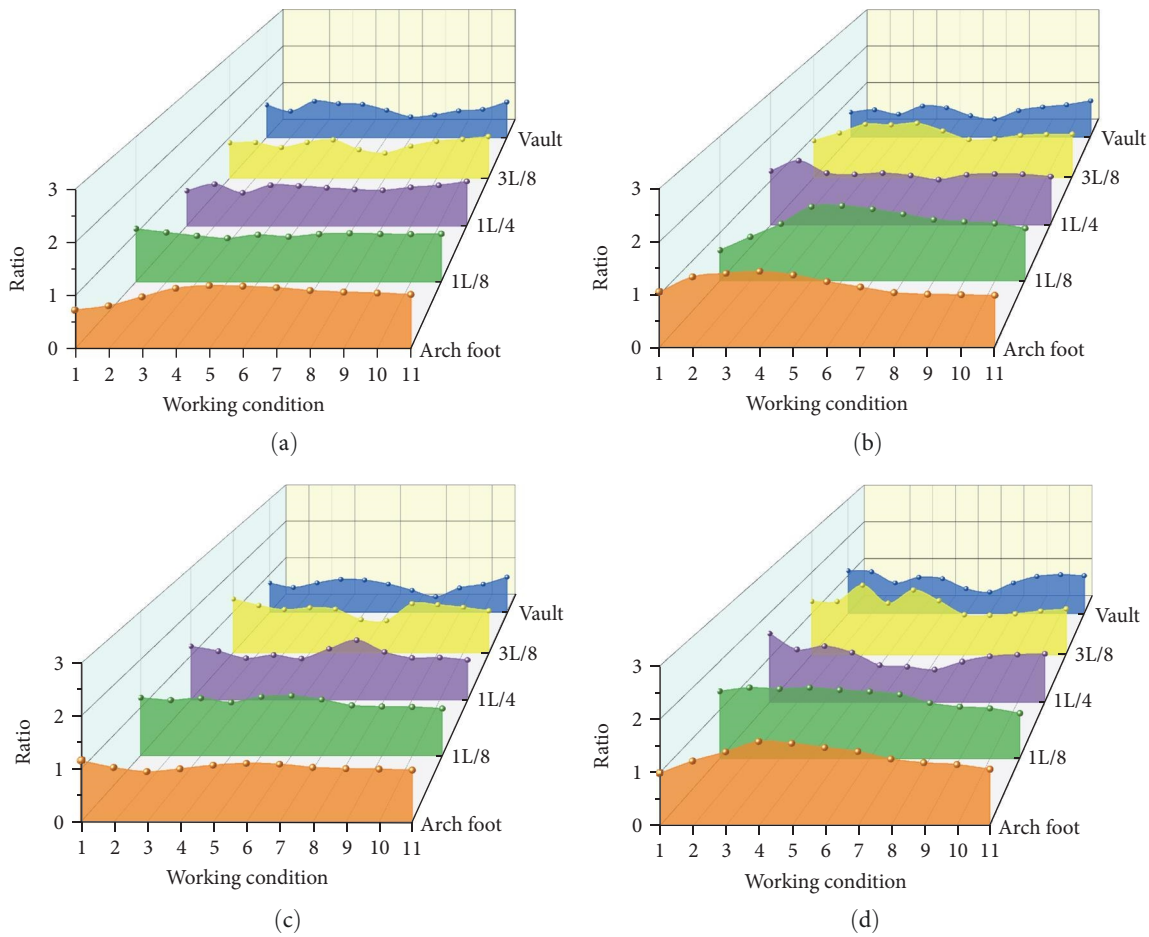

FIGURE 7: Axial force ratio diagram of chord excited by traveling wave in Y direction: (a) upper chord ($N_{\max}$); (b) lower chord ($N_{\max}$); (c) upper chord ($N_{\min}$); (d) lower chord ($N_{\min}$).

structural acceleration, velocity, and displacement; F_b is the time history force applied to the additional mass point; $\ddot{u}_g$ is the ground acceleration. The subscripts bb, ss, and sb represent the degrees of freedom of the supporting nodes, structural degrees of freedom, and their coupled degrees of freedom.

Extending Equation (1)'s second line produces the following:

$$\boldsymbol{M}_0\,\ddot{u}_b + \boldsymbol{M}_{bb}\,\ddot{u}_b + \boldsymbol{C}_{bb}\dot{u}_b + \boldsymbol{K}_{bb}u_b = \boldsymbol{M}_0\,\ddot{u}_g. \tag{2}$$

Under $\boldsymbol{M}_0 \gg \boldsymbol{M}_{bb}$, the acceleration of the supporting node in Equation (2) is compatible with the input ground acceleration, i.e., $\ddot{u}_b \approx \ddot{u}_g$ when the mass $\boldsymbol{M}_0\,\ddot{u}_g$ is significantly larger than the other elements in the equation, obtaining absolute acceleration input.

The bridge weighs 1.5×10^5 kg in total, plus an extra 1.5×10^{11} kg at the arch node. This is achieved by releasing three orthogonal translational degrees of freedom and applying a time history force $\boldsymbol{M}_0\,\ddot{u}_g$ in the corresponding direction.

The acceleration time history of seismic waves can be transformed into an external force time history by building a dynamic finite element model with mass nodes. To calculate the structural reaction to nonuniform inputs, seismic waves of the same type, with various arrival timings or with distinct site types, might be input at separate support points.

3.2. Traveling Wave and Combined Site Input. Longitudinal bridge input in the horizontal plane, or a displacement difference Li on the bridge axis, is typically taken into account when discussing the nonuniform input of large-span bridges. On the other hand, traveling wave effects might affect the bridge's horizontal and vertical planes due to changes in the relative positions of the source and the bridge space. Seismic waves and their propagation medium are highly unpredictable. As illustrated in Figure 4, the seismic input displacement differential Li will fluctuate if the seismic source is able to shift in a transverse, vertical, and horizontal plane around the bridge's arch foot. Nonetheless, the rate at which various media propagate at various locations also varies. Consequently, in each of the three orthogonal planes of space, there will be a traveling wave displacement difference. The input displacement difference between the horizontal and vertical directions of the bridge can also be investigated based on the values along the bridge direction because the same set of recorded waves is orthogonal.

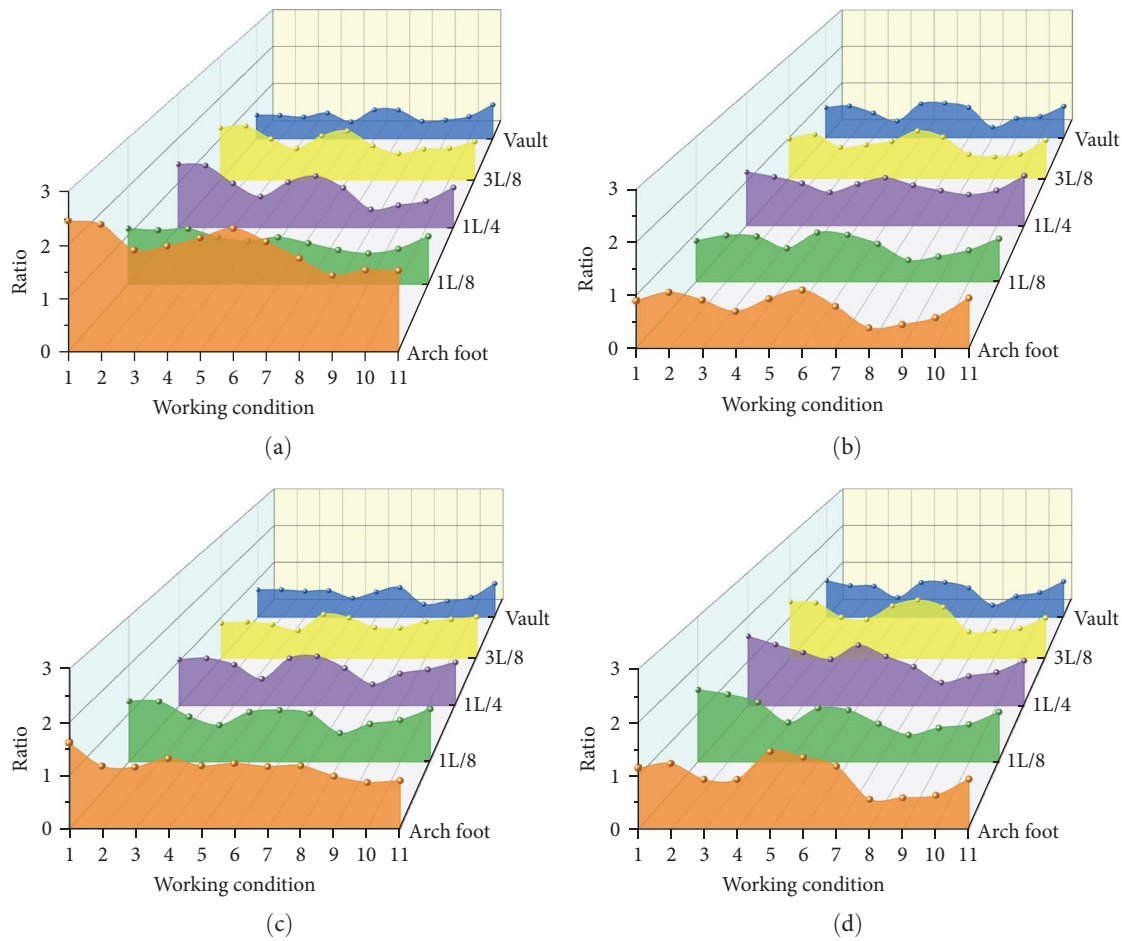

Figure 8: Axial force ratio diagram of chord excited by traveling wave in Z direction: (a) upper chord (N_{max}); (b) lower chord (N_{max}); (c) upper chord (N_{min}); (d) lower chord (N_{min}).

When a long-span arch bridge has a fragile soil base on one side, the composite structure is employed. The nonuniform input of the long-span arch bridge site under the combined site conditions is a design condition since the two arches of the structure are positioned in various types of sites. Consequently, the nonuniform inputs in the combined field are studied along with the traveling waves in the X (longitudinal), Y (transverse), and Z (vertical) directions.

3.3. Seismic Wave Selection. Waves collected by EL Centro are chosen as the input waves for the traveling wave impacts analysis based on the availability of strong earthquake recordings. For the combined site effect analysis, typical recorded waves from EL Centro, Taft, Hollywood, and San Fernando were chosen as input waves based on the categories of hard soil, medium hard soil, soft soil, and soft soil sites. The peak acceleration value in the main direction is corrected by amplitude, and the unified correction value is applied for other directions based on the effective peak acceleration of 0.415 with a 2% likelihood of exceedance (E2 level) in the seismic safety assessment for 50 years. Table 1 displays the peak acceleration correction values, and Figure 5 displays the corrected EL Centro 3D seismic waves.

4. Multiway Traveling Wave Effect

The corrected 3D EI Centro recorded waves are input at the arch node for analysis, and the structural reaction is computed using the mass multipoint input time history analysis method. Twelve types of apparent wave velocities are chosen, namely 150, 200, 250, 375, 500, 650, 800, 1,200, 1,600, 2,000, 4,000, and ∞ (i.e., uniform input), based on the typical shear wave velocities divided by site type. Table 2 displays the hysteresis time at the input position. The hysteresis time t is determined by dividing the apparent wave velocity by the input displacement difference.

The chord produces alternating tension and pressure during an earthquake, and the structural reaction values are separated into two working conditions for discussion: N_{max} and N_{min}. For structural design purposes, the equivalent envelope value can be utilized, as the tension is positive and the compression is negative.

4.1. Axial Force Response. Variable n is defined as the ratio of axial force between traveling wave input and uniform input to make comparison and explanation of changes in structural response easier. As indicated by Table 2, a total of 11

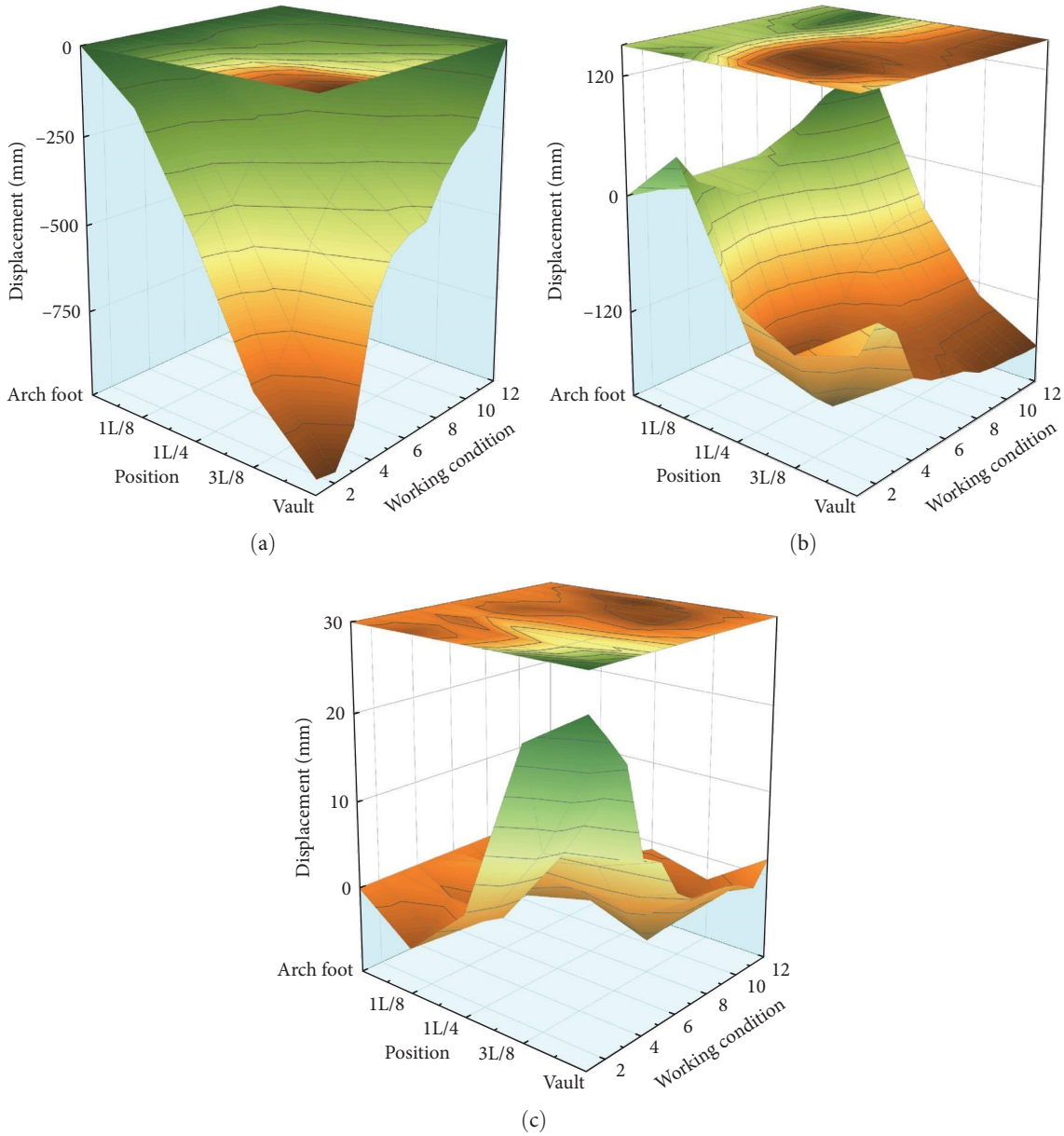

Figure 9: Displacement diagram of chord under traveling wave excitation: (a) Z-direction displacement under X-direction input; (b) Y-direction displacement under Y-direction input; (c) Z-direction displacement under Z-direction input.

Table 3: Combined site input table.

Working condition	1	2	3	4	5	6	7	8	9	10
Input combination	E–E	E–T	E–H	E–S	T–T	T–H	T–S	H–H	H–S	S–S

operating conditions were examined; the uniform input is found in operating condition 12.

Figures 6–8 show that the axial force ratio fluctuates randomly with two or more peaks under the X-direction traveling wave input, but overall, it is greater than 1. The arch crown section's maximum axial force ratio is 8.2, while the maximum value of the other sections is approximately 6. Under design circumstances, the arch crown's maximum axial force ratio is 6.26. The axial force ratio fluctuates with apparent wave speed in a smooth manner under the Y-direction traveling wave input. There is also some randomness in the fluctuation of the axial force ratio between the upper and lower chords of the same section under various working conditions; it can vary from a minimum of 0.51 to a maximum of 1.56. Under the design working condition L/8, the maximum axial force ratio is 1.27. With three or

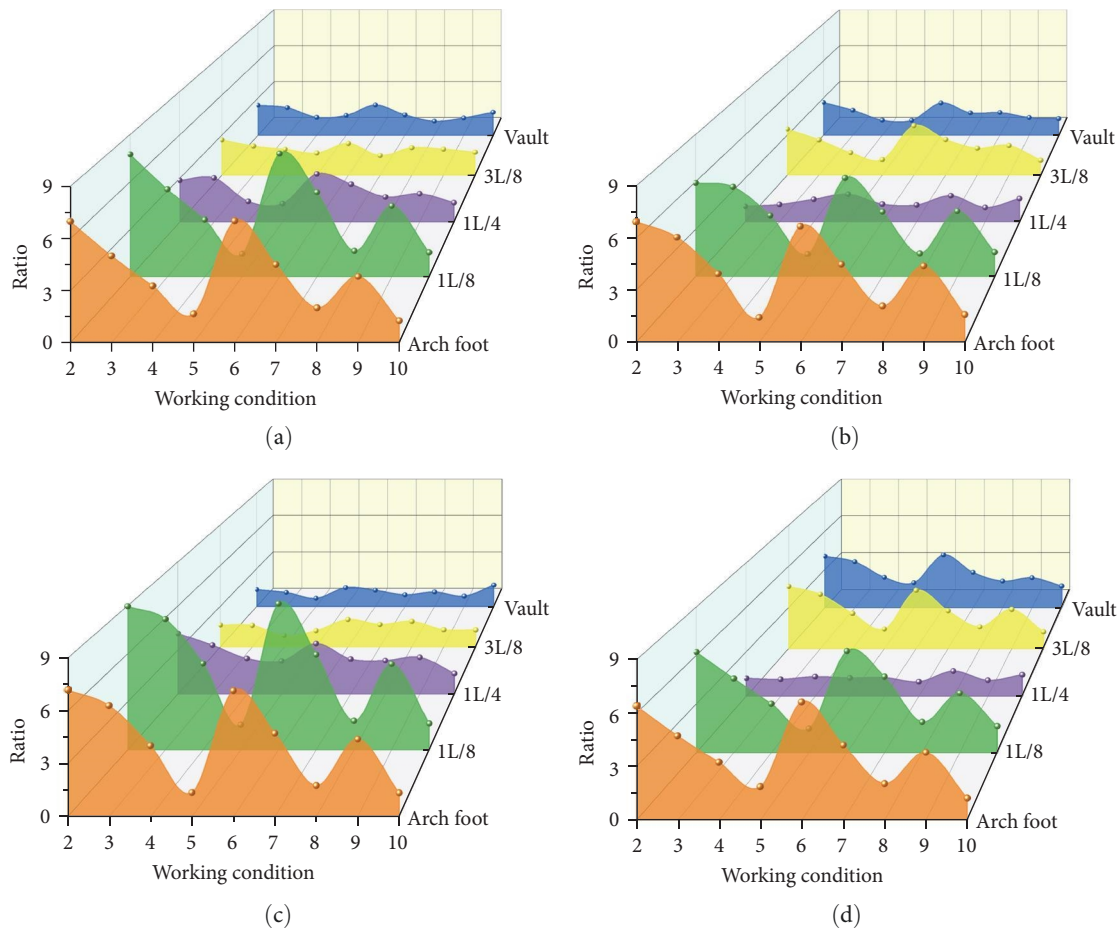

Figure 10: Axial force ratio diagram of chord excited by local field incentives in X direction: (a) upper chord (N_{max}); (b) lower chord (N_{max}); (c) upper chord (N_{min}); (d) lower chord (N_{min}).

more peaks, the random variation of the chord axial force ratio with the change in apparent wave speed is more noticeable under the Z-direction traveling wave input. Every sector has a somewhat steady trend of changes, with a maximum value of 2.45 and a minimum value of 0.57. Under design settings, the arch foot's maximum axial force ratio is 1.75.

Overall, the axial force ratio greatly alters and is impacted by the X-direction traveling wave input; the axial force ratio varies rather smoothly under the Z- and Y-direction traveling wave input and the arch foot section has a reasonably large influence; the response shows spatial heterogeneity.

4.2. Displacement Response. The bending moment of a single chord cannot accurately represent the total bending impact of the main arch because this bridge is a variable cross-section truss arch structure. Given that the displacement changes of the upper and lower chords under the N_{max} and N_{min} working conditions under unidirectional seismic input are comparatively comparable, the bending moment changes are reflected by the upper chord displacement under the N_{min} working condition. Analyze the displacement in the Z direction under the X and Z direction input, and analyze the displacement in the Y direction under the Y direction input.

The data presented in Figure 9 illustrates that, under the traveling wave in the X-direction, the displacement of the arch foot towards the arch crown increases gradually as the apparent wave velocity decreases, leading to a rapid increase in the arch crown with a significant displacement impact; in the Y-direction, the displacement of the arch foot toward the arch crown first decreases and then increases, with a significant effect of L/4–3L/8 in the 200–500 m/s range; in the Z-direction, the displacement changes randomly, and the L/8–arch crown rapidly increases when it changes from 200 to 800 m/s; the displacement response exhibits spatial variability, and the displacement of the arch crown under design conditions in the X and Z directions has increased about two times.

5. Combined Site Effects

The E–E, T–T, H–H, and S–S operating conditions are four identical site inputs, while the other combinations are combined inputs from separate sites, it is to input seismic waves of different site types to the arch. The combined site inputs are displayed in Table 3.

5.1. Axial Force Response. The standard value (condition 1) is the axial force value under the same input of EI Centro; the

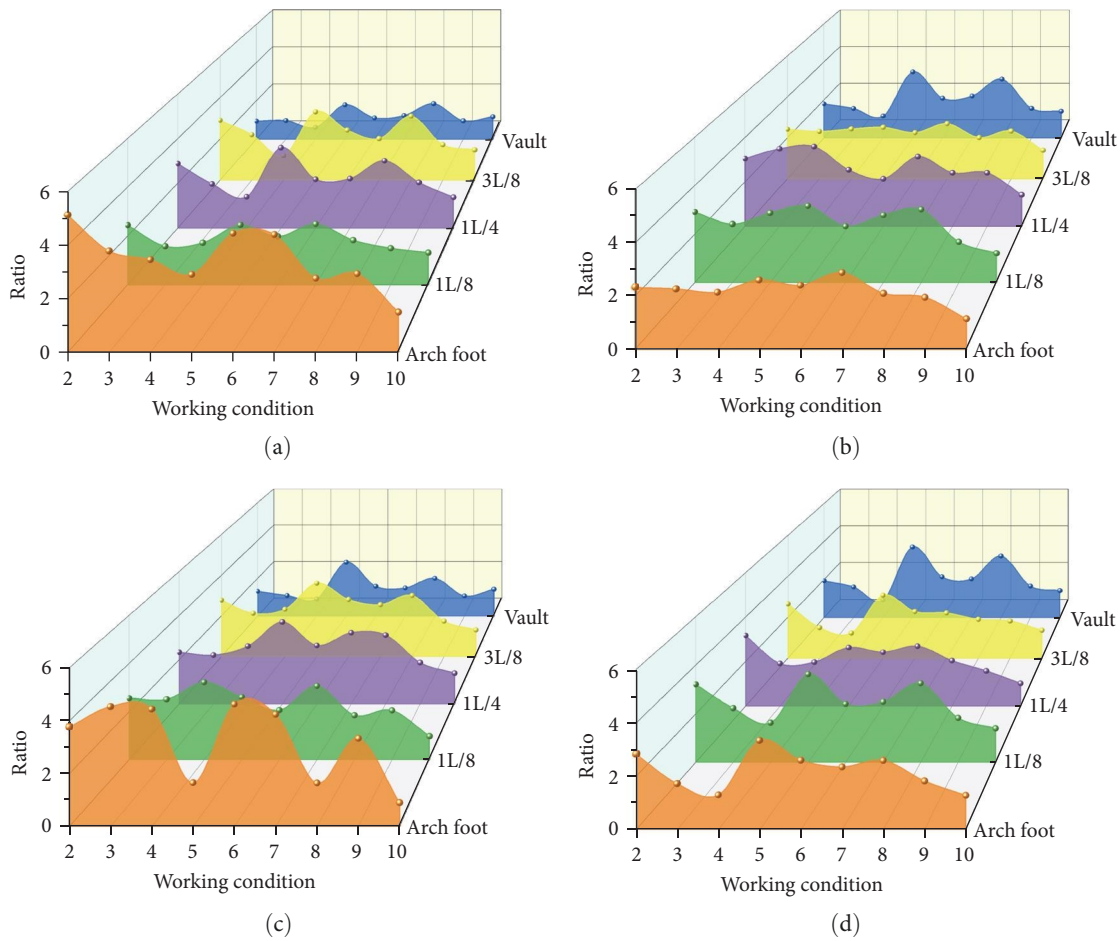

Figure 11: Axial force ratio diagram of chord excited by local field incentives in Y direction: (a) upper chord (N_{max}); (b) lower chord (N_{max}); (c) upper chord (N_{min}); (d) lower chord (N_{min}).

variable n is defined as the ratio of the axial force value under different combined inputs to the standard value. There are nine different working conditions, as shown in Table 3, and the mass multipoint input time history analysis approach is used to determine the structural reaction.

As seen in Figures 10–12, it is evident that:

(1) The axial force ratio of the L/8 section and arch foot changes dramatically under the input in the X direction, reaching maximum values of 6.9 and 7.6. In other parts, the changes are more gradual.

(2) Each chord segment's axial force ratio dramatically increases in response to Y-direction input, with the arch foot section exhibiting the highest value of 5.13.

(3) The axial force ratios of the L/4 and 3L/8 sections vary relatively smoothly, with the arch crown section showing the largest shift at 8.34, whereas the axial force ratios of the arch foot, L/8, and arch crown sections change dramatically under the Z-direction input.

Overall, the axial force ratio under the three orthogonal directions of uniform input is reasonably similar, following the same amplitude modulation of seismic waves for various site types, as indicated by the position of the wave trough in the figure. The axial force ratio is greater than 1 under the other input combinations; the axial force ratio varies at a relatively consistent pace at each chord section, but the amplitude of variation varies randomly under different input combinations; the overall changes occur in three bands, with peaks at the input of adjacent combinations; the axial force difference between the combined input lower chord is less the softer the soil on the site.

5.2. Displacement Response. How the top chord's displacement varies when a single direction local field is paired with N_{min} working condition is examined. The Z-direction displacement under the input of X and Z directions and the Y-direction displacement under the input of Y directions are analyzed.

Figure 13 illustrates this; when input is applied in the X direction, the arch foot's direction towards the arch crown

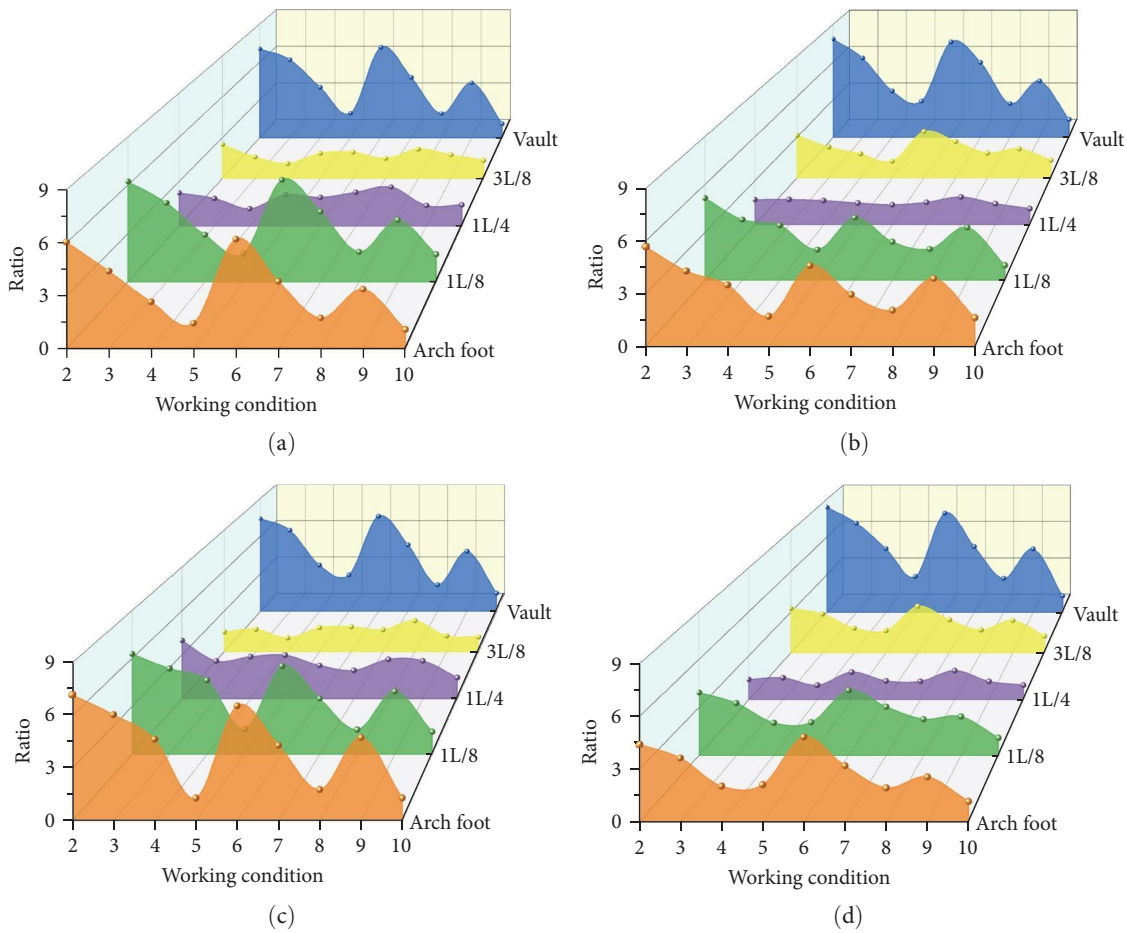

FIGURE 12: Axial force ratio diagram of chord excited by local field incentives in Z direction: (a) upper chord (N_{max}); (b) lower chord (N_{max}); (c) upper chord (N_{min}); (d) lower chord (N_{min}).

exhibits a periodic change with the input transformation of the combined site; however, the amplitude increases quickly, and the arch crown's displacement has a significant impact; when input is applied in the Y direction, the arch foot's change to the L/8 section is gentle, but the L/8 to the arch crown section exhibits a periodic increase in amplitude, and the arch crown's displacement has a significant impact; When input is applied in the Z direction, the L/4 to arch crown section displays a periodic increase in amplitude, which increases quickly in the combination of medium to weak fields and has a significant impact.

6. Conclusion

(1) Large-span structures have nonuniform seismic input circumstances of traveling waves and uneven sites in both horizontal and vertical inputs. Seismic waves and propagation medium are also random. The axial force ratio and displacement changes of each chord segment under different operating circumstances have spatial features when the input is nonuniform.

(2) When the amplitude modulation is applied evenly to various recorded waves, the axial force of the lower chord is identical. The chord's axial force ratio varies randomly and periodically in response to traveling wave input. It is not true that the axial force ratio increases with increasing lag time; rather, the axial force ratio varies substantially with input in the X direction and is relatively gradual with input in the Y and Z directions. The axial force of the arch rib is significantly affected by the traveling wave input.

(3) The displacement of the arch foot toward the arch crown increases gradually with the decreasing apparent wave velocity under the input of traveling waves in the X and Z directions, with the arch crown displacement having the greatest influence under the Y-direction traveling wave input, the L/4–3L/8 segment has a significant influence, initially decreasing and then increasing; under the unidirectional traveling wave input, each displacement change exhibits a specific trend, but the changing trends in the three directions are inconsistent.

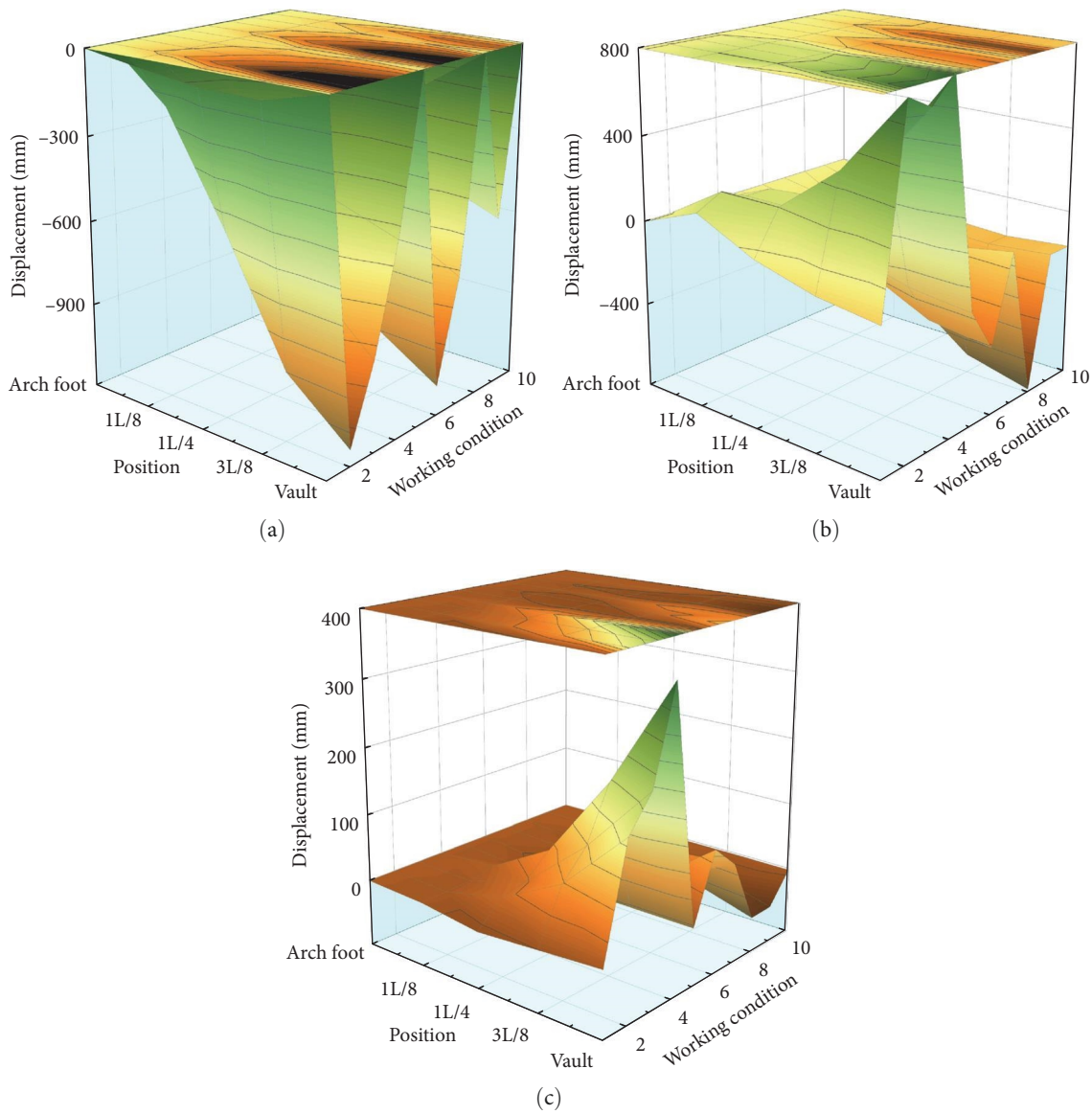

Figure 13: Displacement diagram of chord under local field incentives: (a) Z-direction displacement under X-direction input; (b) Y-direction displacement under Y-direction input; (c) Z-direction displacement under Z-direction input.

(4) The axial force ratio varies at a reasonably consistent pace under single-direction combined field inputs, and it varies at a somewhat random pace at each section under different-direction combined field inputs; the axial force ratio changes significantly and significantly impacts the system.

(5) The displacement of the chord increases gradually under the nonuniform input of the combined site, from the arch foot to the arch crown, with the arch crown being the most significant; the displacement change amplitude increases sequentially when the hard field transforms into the weak field, and the influence of the weak field is significant; and the displacement continuously increases when the hard field transforms into the weak field following the same amplitude modulation input of seismic waves from various types of sites.

The horizontal and vertical traveling wave effects of large-span deck steel tube concrete arch bridges are inconsistent under high seismic region building conditions, the axial force of the chord increases significantly in different sites of the arch, and the adaptation selection of arch bridges should be carefully examined.

Data Availability

If necessary, please contact the author to provide relevant data.

Conflicts of Interest

The authors declare that they have no conflicts of interest.

Acknowledgments

This study was funded by the National Natural Science Foundation of China (51768037, 52162043) and the Key R&D Projects in Gansu Province of China (22YF7GA043, 22YF11GA301).

References

[1] K. Z. Xie, *Seismic Analysis and Evaluation Method of CFST Arch Bridge*, China Construction Industry Press, Beijing, 2017.

[2] J. L. Zheng and J. J. Wang, "Concrete-filled steel tube arch bridges in China," *Engineering*, vol. 4, no. 1, pp. 143–155, 2018.

[3] C. H. Y. Shao, *Modern Arch Bridge*, China Communications Press, Beijing, 2021.

[4] K. Fan, *Experimental Study and Theoretical Analysis of Multi-Dimensional and Multi-Point Seismic Response of Large-Span Structures*, Beijing University of Technology, Beijing, 2008.

[5] M. T. Stephens, D. E. Lehman, and C. W. Roeder, "Seismic performance modeling of concrete-filled steel tube bridges: tools and case study," *Engineering Structures*, vol. 165, pp. 88–105, 2018.

[6] C. F. Liao, P. Ouyang, and F. Y. Luo, "Scheme comparison of arch abutment foundation on north bank of the Pingnan Third Bridge," *Chinese and Foreign Highways*, vol. 34, no. 6, pp. 157–160, 2021.

[7] B. Song, H. B. Yi, and H. Y. Zhou, "Seismic response analysis for long-span arch bridges under consideration of traveling wave effect," *Journal of Beijing University of Technology*, vol. 37, no. 3, pp. 375–380, 2011.

[8] C. Su and H. B. Chen, "Seismic response of long-span bridge under multi-support excitation," *Journal of South China University of Technology (Natural Science Edition)*, vol. 36, no. 11, pp. 101–107, 2008.

[9] Y. L. Zhang, Y. Wang, X. C. Chen, L. S. Yu, and C. C. Liu, "Spatial seismic response of long-spandeck rail way steel truss arch bridge under multi-dimensional excitation," *China Railway Science*, vol. 41, no. 5, pp. 56–63, 2020.

[10] S. J. Tong, X. Wu, and G. Li, "Analysis of seismic traveling wave effect on long span concrete-filled steel tube arch bridges," *Bridge Construction*, no. 2, pp. 27–30, 2008.

[11] Y. J. Chen, D. Y. Zhang, and X. Li, "Stochastic seismic analysis of a CFST arch bridge under spatially varying groundmotions," *Engineering Mechanics*, vol. 30, no. 12, pp. 99–106, 2013.

[12] H. Wang, F. F. Li, and Z. H. Zong, "Analysis of seismic traveling wave effect of long-span CFST arch bridge," *Journal of Vibration Engineering*, vol. 25, no. 5, pp. 556–563, 2012.

[13] Z. M. Hu, J. Y. Li, and T. Y. Huang, "Seismic response analysis of concrete-filled steel tube arch bridge based on traveling wave effect," *Bridge Construction*, no. 1, pp. 25–28, 2010.

[14] L. X. Wang, Q. Y. Liu, and S. K. Di, "Analysis of stationary random seismic response of arch bridge with concrete-filled steel tubes under non-uniform excitation," *Journal of Lanzhou University of Technology*, vol. 42, no. 2, pp. 124–129, 2016.

[15] B. Li and N. Chouw, "Experimental investigation of inelastic bridge response under spatially varying excitations with pounding," *Engineering Structures*, vol. 79, pp. 106–116, 2014.

[16] X. Z. Li, D. H. Yang, K. N. Lei, L. Xiao, and S. Y. Dai, "Seismic response of continuous beam-arch bridge under spatially varying ground motions," *Journal of Southwest Jiaotong University*, vol. 56, no. 2, pp. 221–228, 2021.

[17] K. M. Bi, H. Hao, and W. X. Ren, "Seismic response of a concrete filled steel tubular arch bridge to spatially varying ground motions including local site effect," *Advances in Structural Engineering*, vol. 16, no. 10, pp. 1799–1817, 2013.

[18] J. Ma and Y. Li, "Analysis of traveling wave effect on half-through CFST arch bridge by large mass method," *Key Engineering Materials*, vol. 540, pp. 21–28, 2013.

[19] Z. Y. Li, P. P. Dang, and D. J. Mu, "MR damper semiactive control for bridge under multi-support seismic excitation," *Applied Mechanics and Materials*, vol. 90-93, pp. 1402–1405, 2011.

[20] K. Soyluk, "Comparison of random vibration methods for multi-support seismic excitation analysis of long-span bridges," *Engineering Structures*, vol. 26, no. 11, pp. 1573–1583, 2004.

[21] W. T. Gong, H. P. Yang, and L. I. Jing, "Analysis of seismic response regularity of stiff skeleton concrete arch bridge under traveling wave effect," *Journal of Southwest Jiaotong University*, vol. 60, no. 2, pp. 35–39, 2020.

[22] S. Farahmand-Tabar and M. Barghian, "Seismic assessment of a cable-stayed arch bridge under three-component orthotropic earthquake excitation," *Advances in Structural Engineering*, vol. 24, no. 2, pp. 227–242, 2020.

[23] Z. Li, G. Wang, J. Fan, W. Wu, Y. Jian, and X. Li, "Seismic response analysis of multidimensional and multiangle long-span top-supported CFST arch bridge," *Advances in Civil Engineering*, vol. 2022, Article ID 6807916, 13 pages, 2022.

[24] J. L. Zheng, *Innovative Technology for 500-Meter Scale Concrete-Filied Steel Tubular Arch Bridges*, Shanghai Science and Technology Press, Shanghai, 2020.